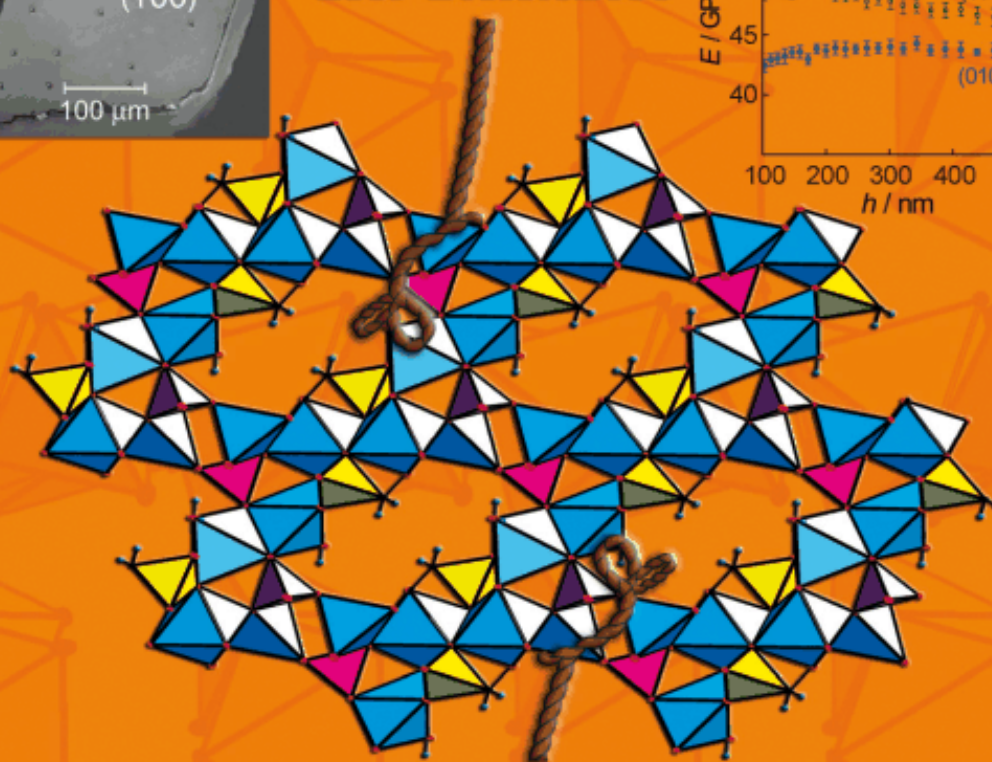
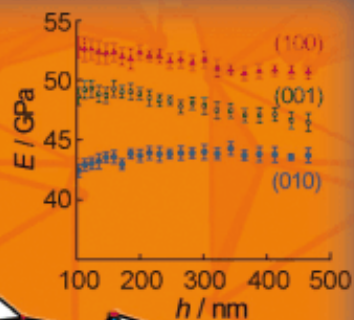


A EUROPEAN JOURNAL

**CHEMPHYSICHEM**

OF CHEMICAL PHYSICS AND PHYSICAL CHEMISTRY

**EXPERIMENT****THEORY**

$$\varepsilon_{ij} = S_{ijkl} \sigma_{kl}$$

**11/2010**

A Journal of

**Reviews:** Quantum-Dot-Sensitized Solar Cells

(S. Rühle, A. Zaban, and M. Shalom)

**Highlights:** Aqueous Carbonic Acid

(T. Loerting and J. Bernard)

www.chemphyschem.org

## Probing the Mechanical Properties of Hybrid Inorganic–Organic Frameworks: A Computational and Experimental Study

Monica Kosa,<sup>\*,[a]</sup> Jin-Chong Tan,<sup>[b]</sup> Crystal A. Merrill,<sup>[b]</sup> Matthias Krack,<sup>[c]</sup> Anthony K. Cheetham,<sup>\*,[b]</sup> and Michele Parrinello<sup>[a]</sup>

Hybrid framework materials are modular compounds consisting of metal ions and organic linkers, variation of which has given rise to a myriad of structures with technologically relevant properties. To date, extensive experimental and theoretical studies have been carried out to understand key factors that affect processes such as gas adsorption, gas separation and heterogeneous catalysis in nanoporous metal-organic frameworks (MOFs).<sup>[1]</sup> Dense hybrid frameworks are also of growing interest on account of their unique physical properties, such as multiferroics, electronic conductivity and photoluminescence, among others.<sup>[2]</sup> For all viable applications, the robustness of the materials and, in particular, a detailed understanding of their mechanical properties, are necessary for successful utilization. This field, however, remains largely unexplored. Recent experimental studies<sup>[3]</sup> have demonstrated that the elastic properties, especially the bulk modulus ( $B$ )<sup>[4]</sup> and the Young's modulus ( $E$ )<sup>[5]</sup> of nanoporous and dense hybrid frameworks, can be correlated to their density, dimensionality and their underlying chemical structures. In addition, recent computational studies have reported that the bulk moduli of a family of isoreticular metal-organic frameworks (IRMOFs) depend on the size of the aromatic organic linkers (which determines the density).<sup>[6]</sup> Herein, we employed a combination of computational and experimental approaches to probe the elastic properties of a dense and anisotropic hybrid framework material: zinc phosphate phosphonoacetate hydrate,  $Zn_3-(PO_4)(O_2CCH_2PO_3)(H_2O)_3$ , **1**.<sup>[7]</sup> We propose an efficient computational scheme for the approximate analysis of the Young's modulus and the Poisson's ratio ( $\nu$ ) along the principal directions of an anisotropic crystal. Notably, this approach circumvents the intricacies involved in computing the full elastic stiffness tensor.<sup>[8]</sup> The validity of our theoretical calculations was confirmed by single-crystal nanoindentation experiments. In

addition, theoretical studies were performed by subjecting the anisotropic framework to hydrostatic compression to reveal the role of the basic building blocks.

Studies to date indicate that both the local density approximation (LDA) and the general gradient approximation (GGA) levels of density functional theory (DFT) have over-predicted the bulk modulus ( $B$ ) of MOF materials. By way of an example, the  $B$  value of the lightweight MOF-5 (density of  $0.59 \text{ g cm}^{-3}$ ) was calculated to be in the range of 16–20 GPa,<sup>[6]</sup> which is notably higher than measurements obtained from other related MOF-type structures of considerably higher densities. Specifically, high pressure experiments have determined  $B$  values at only 6.5 GPa ( $0.93 \text{ g cm}^{-3}$ ) and 14 GPa ( $1.54 \text{ g cm}^{-3}$ ) for MOF materials with zeolitic imidazolate framework (ZIF) structures.<sup>[3c,9]</sup> Likewise, a large discrepancy exists in terms of the Young's modulus ( $E$ ). Theoretical studies on cubic crystals of MOF-5 have reported  $E$  values in the range of 14.8–21.6 GPa,<sup>[6a,b]</sup> whereas the measured value is almost an order of magnitude lower at 2.7 GPa.<sup>[6a]</sup> Such a discrepancy was attributed to the physical degradation of the crystals and indentation measurements associated deficiencies.<sup>[6a]</sup> Here, it is worth noting that having zinc–oxygen cores,<sup>[6b,e]</sup> the electronic structure of MOF-5 is reminiscent of that of bulk ZnO. Various computational studies on the elastic properties of ZnO have revealed a large spread and inconsistencies in the calculated data, probably as a result of various implementation schemes of the DFT/pseudo-potential method [see Table S7 in the Supporting Information (SI) for details]. This is yet, another manifestation of the deficiency of traditional LDA or GGA approximations to correctly describe strongly correlated systems and sensitivity of the calculated elastic properties data to the computational method, even on a qualitative scale.

The asymmetric unit of **1** (Figure 1A) shows that there are three crystallographically distinct Zn sites. Zn1 is six-coordinated with a distorted  $ZnO_6$  octahedron, Zn2 is in a distorted  $Zn(H_2O)_4$  trigonal bipyramid, and Zn3 is in a  $ZnO_4$  tetrahedron. **1** has a 3-D framework structure made up of 2D Zn–O–Zn connectivity with a complex pillared structure (Figure 1B). The layers contain chains made up of dimers of edge-shared Zn1 zinc oxide octahedra that are linked by corner-sharing in the  $a$ -direction by Zn3 tetrahedra (Figure 1C); these chains are connected in the  $bc$ -plane by dimeric  $(Zn_2)_2O_8$  units to form the Zn–O–Zn layers. The Zn–O–Zn layers are connected by phosphate groups bridging  $ZnO_4$  tetrahedra, and these bridges section off small “channels” that run parallel to the  $a$ -axis (Figure 1B). It is noted that although there is no accessible porosity in this structure, there is a small void space present within

[a] Dr. M. Kosa,<sup>+</sup> Prof. M. Parrinello  
Computational Science  
Department of Chemistry and Applied Biosciences, ETH Zürich  
c/o USI Campus, Via Giuseppe Buffi 13, 6900 Lugano (Switzerland)  
Fax: (+41) 586664817  
E-mail: monica.kosa@phys.chem.ethz.ch

[b] Dr. J.-C. Tan,<sup>+</sup> Dr. C. A. Merrill, Prof. A. K. Cheetham  
Department of Materials Science and Metallurgy  
University of Cambridge, Pembroke Street  
Cambridge CB2 3QZ (UK)  
E-mail: akc30@cam.ac.uk

[c] Dr. M. Krack  
Paul Scherrer Institut, 5232 Villigen PSI (Switzerland)

[<sup>+</sup>] These authors contributed equally to this work.

Supporting information for this article is available on the WWW under <http://dx.doi.org/10.1002/cphc.201000362>.

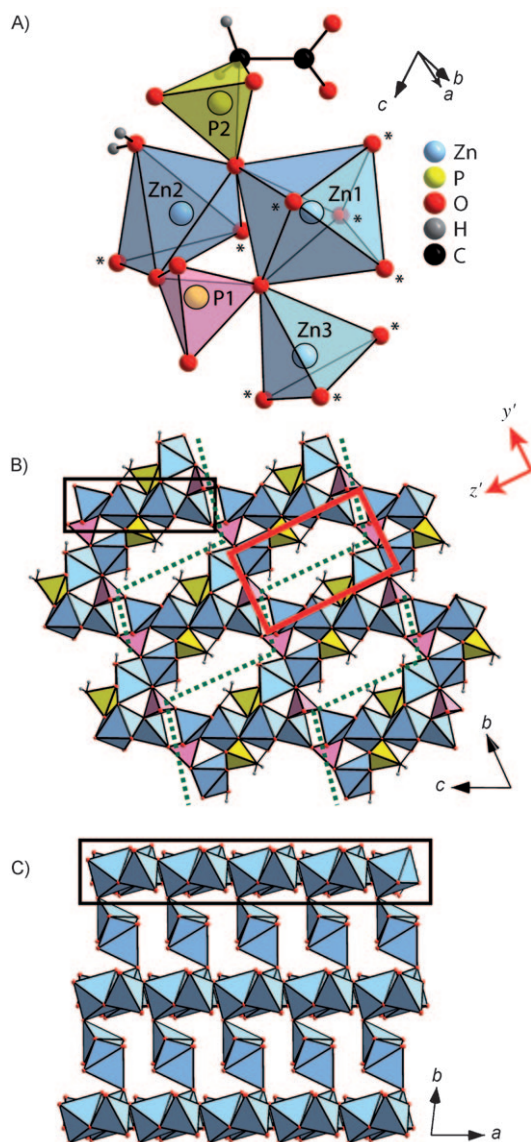


**Figure 1.** The crystal structure of **1**,  $\text{Zn}_3(\text{H}_2\text{O})(\text{PO}_4)(\text{O}_2\text{CCH}_2\text{PO}_3)$ . A) The asymmetric unit, wherein the zinc polyhedra are in blue,  $\text{PO}_4$  tetrahedron is in pink and  $\text{PCO}_3$  tetrahedron in yellow. Atoms denoted with an asterisk are included to complete the metal polyhedra. B) View of the “channels” oriented along the  $a$ -axis. The adjacent Zn–O–Zn layers are highlighted by the green dotted lines while a  $\text{ZnO}_x$  ribbon is outlined in black. The red outline encloses an elliptical cavity and designates the pseudo-orthorhombic unit cell **1'**, associated with the  $y'$ - and  $z'$ -axes. C) View of the  $\text{ZnO}_x$  layered structure down the  $c$ -axis, whereby the ribbon outlined in black corresponds to that of B. Note that  $\text{PO}_4$  and  $\text{PCO}_3$  tetrahedra are omitted for clarity.

the channels. It is demonstrated herein how the morphology of this void space affects the anisotropic elastic properties of **1**.

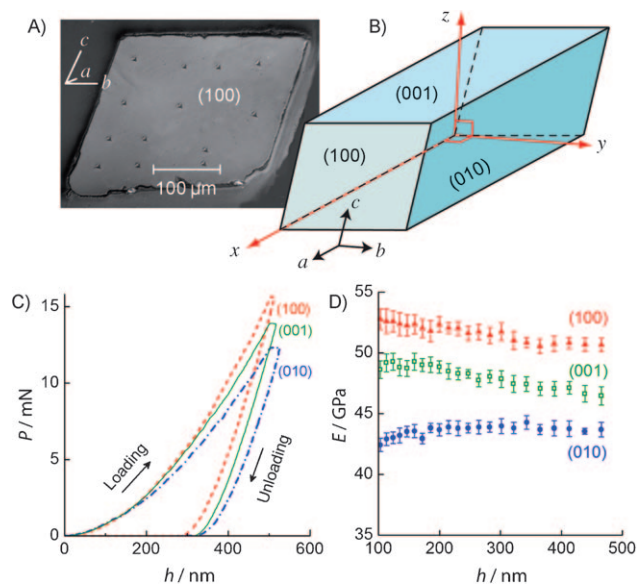
The optimized geometry and cell parameters of **1** calculated at 0 K are summarized in Table 1. The DFT calculations agree well with the experimentally determined structure, albeit with an overestimation of the cell parameters of  $\sim 1$ – $2\%$ . This trend is common for the PBE functional in general,<sup>[10]</sup> and is also reflected when applied to MOF structures.<sup>[11]</sup> Using the optimized structure of **1** as the starting geometry, we then calculated its bulk modulus<sup>[12]</sup> and found that  $B=48.6$  GPa. This is markedly

Table 1. Comparison between measured and calculated unit cell dimensions of <b>1</b> .		
Unit cell parameters	Experimental	DFT calculation <sup>[a]</sup>
Lengths [Å]		
$a$	$4.90930(10)$	5.012
$b$	$9.5271(2)$	9.709
$c$	$11.1246(3)$	11.393
Angles [°]		
$\alpha$	$64.8130(10)$	64.355
$\beta$	$82.915(2)$	82.863
$\gamma$	$81.068(2)$	80.756
Volume [Å <sup>3</sup> ]	$464.179(18)$	492.34
Density [g cm <sup>-3</sup> ]	3.19	3.01

<sup>[a]</sup> Computation performed on a  $2 \times 1 \times 2$  cell, which corresponds to  $a=10.024$  Å,  $b=9.709$  Å,  $c=22.786$  Å and a cell volume of  $1969.34$  Å<sup>3</sup>. The calculated dimensions are normalized to obtain a  $1 \times 1 \times 1$  cell, as listed here.

higher than the calculated values for porous MOF-5 (e.g.  $B=16.3$  GPa),<sup>[3d]</sup> reflecting the fact that porous hybrid frameworks are more compressible; this is consistent with the large difference observed between their measured densities, that is,  $3.19$  g cm<sup>-3</sup> for **1** compared with  $0.59$  g cm<sup>-3</sup> for MOF-5.

It has recently been reported that hybrid framework materials can exhibit highly anisotropic mechanical properties in view of their complex chemical topology.<sup>[3a,b]</sup> As shown in Figure 2, we confirmed via nanoindentation experiments that the Young's moduli of **1** are indeed anisotropic along the primary crystallographic orientations. This is not surprising by virtue of the complex chemical topology of **1**, as highlighted above, and also given its triclinic crystal structure. Neverthe-



**Figure 2.** Single-crystal morphology and nanoindentation data of **1**. A) The (100) facet showing residual indents made by a three-faced pyramidal diamond tip. B) Schematic of the crystal showing its low index faces and orientations of the triclinic cell. C) Representative load vs displacement curves obtained by indenting (to 500 nm) normal to the (100)-, (001)- and (010)-oriented facets. D) The corresponding Young's moduli ( $E$ ) as a function of depth, extracted from the  $P$  vs  $h$  curves.

less, we note that DFT calculation on the anisotropic elastic properties of hybrid framework has never been attempted previously. Herein (Table 2), we found that the calculated and ex-

	Single-crystal nanoindentation <sup>[a]</sup>	DFT calculation <sup>[b]</sup>				
Young's modulus, $E$ (GPa)	$E_{(100)}$	$53.34 \pm 1.50$	$E_x$	74.56		
	$E_{(010)}$	$42.57 \pm 0.93$	$E_y$	55.44		
	$E_{(001)}$	$49.59 \pm 1.32$	$E_z$	61.51		
Poisson's ratio, $\nu_{ij}^{[c]}$	Not measured		$\nu_{xy}$	0.26	$\nu_{yx}$	0.19
			$\nu_{xz}$	0.35	$\nu_{zx}$	0.29
			$\nu_{yz}$	0.37	$\nu_{zy}$	0.29

<sup>[a]</sup> Mean values determined from indentation depths of 100 nm to 500 nm, as shown in Figure 2D. The standard deviation refers to 15 separate indents. <sup>[b]</sup> The  $x$ -,  $y$ - and  $z$ -directions correspond to the Cartesian axes depicted in Figure 2B. <sup>[c]</sup>  $\nu_{ij}$  is defined as the negative ratio of transverse strain to longitudinal strain, that is,  $-\varepsilon_j/\varepsilon_i$ .

perimental anisotropy ratios pertaining to the Young's moduli are  $E_x:E_y:E_z=1.34:1.00:1.11$  and  $E_{(100)}:E_{(010)}:E_{(001)}=1.25:1.00:1.16$ , respectively. The relative stiffnesses, calculated using the proposed scheme (details in the SI) are in good agreement with the experiments. Here, it is noted that the measurements performed normal to the (100)-, (010)- and (001)-oriented facets, as depicted in Figure 2B,<sup>[13]</sup> give good approximations to the properties derived assuming orthogonal  $x$ -,  $y$ -,  $z$ -axes, used in the DFT calculations. Evidently, the  $x$ -axis that is oriented approximately normal to the (100) plane is the stiffest, whereas the  $y$ -direction which is closely related to the normal of the (010) plane appears to be the most compliant (lowest stiffness). In terms of their absolute values, however, the calculated moduli are notably higher than those determined experimentally. In particular, the stiffness measured along the  $x$ -axis has been over predicted by as much as  $\sim 40\%$ , while their magnitudes in the other two orientations are larger by about 25% to 30%. Experimental uncertainties alone (e.g. crystal alignment, surface roughness, indenter tip calibration, etc.) cannot account for such deviations (see SI). In addition, sample degradation cannot be an issue here since the experiments involved freshly synthesized crystals and, unlike many porous MOFs,<sup>[3d]</sup> compound **1** is not moisture sensitive.

From the computational standpoint, the higher stiffnesses obtained from DFT can be attributed to factors arising both from the derivation scheme as well as deficiencies associated with the electronic structure methods used. The currently employed derivation scheme might overestimate the Young's moduli due to the fact that theoretical calculations were performed at 0 K, as opposed to the ambient experimental conditions of about 300 K.<sup>[14]</sup> We note that the overestimation of pressure by DFT and the additional contributions associated with the localized basis set<sup>[15]</sup> might give rise to enhanced stresses as well. Moreover, the incorrect description of the position of the Zn-3d states is known to cause over-hybridization of Zn–O bonds within GGA<sup>[16]</sup> (due to the self-interaction error,

SIE<sup>[17]</sup>). This can further contribute to stiffening of the zinc–oxygen cores. Our preliminary electronic structure calculations (where only the  $\Gamma$ -point of the supercell was included for Brillouin zone integration) indicate that the top of the valence band and the bottom of the conduction band (i.e. HOMO and LUMO orbitals) of **1** exhibit similar structure to that of ZnO and as expected, the band gap of **1** is underestimated.<sup>[18]</sup> We can therefore anticipate that, as with ZnO, the absolute values of the calculated elastic moduli of **1** can be highly sensitive towards the choice of the exchange-correlation functional and the pseudopotential.

In order to study the origin of elastic anisotropy in **1**, we computationally studied its detailed chemical structure under the effects of variable pressures (0 to 5 GPa).<sup>[19]</sup> As shown in Figure 3A, the calculated relative cell parameters under hydrostatic compression indicate that the  $a$ -axis is shortening at the slowest rate (hence of lower strains) while the  $b$ - and  $c$ -axes are contracting at similar rates. We note that the similar mechanical response of the  $b$ - and  $c$ -axes under hydrostatic compression (while the Young's moduli indicate that the  $z$ -axis is relatively stiffer than the  $y$ -axis) can be achieved only if the Poisson's ratios are anisotropic. Indeed the calculated Poisson's

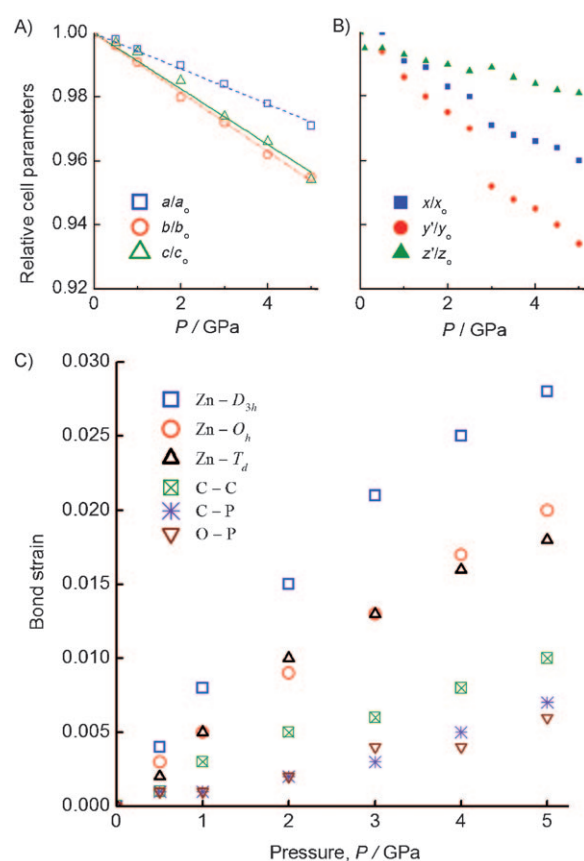


**Figure 3.** Calculated relative cell parameters as a function of hydrostatic pressure of A) a triclinic cell **1**; B) a pseudo-orthorhombic cell **1'**,<sup>[20]</sup> wherein its  $x$ -axis coincides with the  $a$ -axis in **1**. C) Comparison between the bond strains associated with each building block of **1** under hydrostatic compression. The symbols  $D_{3h}$ ,  $O_h$  and  $T_d$  denote trigonal bipyramidal, octahedral and tetrahedral Zn coordination environments, respectively.

ratios found in the range of 0.26–0.37 (see Table 2) confirm such an observation.

To further assess the roles of chemical topology on the elastic anisotropy of **1**, we constructed a pseudo-orthorhombic unit cell, designated as **1'** (red outline in Figure 1B), whereby its *x*-axis corresponds to the *a*-axis in the original triclinic cell, while its *y'*- and *z'*-axes are oriented almost perpendicular to each other. As such, in this computational model, the principal directions of the elliptical cavity are approximately aligned to the principal **1'** cell axes.<sup>[20]</sup> It can be seen in Figure 3B that the *y'*-axis of the pseudo-orthorhombic cell is the most compressible under hydrostatic pressure, whereas the *x*- and *z'*-axes are relatively stiffer. Such a characteristic is consistent with the fact that the *y'*-direction is oriented along the shorter axis of the elliptical cavity and hence is more compressible (and of low stiffness) for geometrical reasons.

The bond strains of each structural building block of **1** as a function of the applied hydrostatic pressure are presented in Figure 3C. Herein, bond strain is defined as the change in the bond length over its original bond distance, and hence a smaller strain signifies a stiffer bond and vice versa. Close examination reveals that the most flexible chemical environments are located around the Zn-*D*<sub>3h</sub> site (probably due to its immediate proximity to the channel), followed by the Zn-*O*<sub>h</sub> and Zn-*T*<sub>d</sub> sites, as indicated by their relatively large strains. Conversely, the C–C, C–P and O–P bond strains are similar to each other, reflecting greater stiffness than the zinc–oxygen cores. The phosphate and phosphonate groups form the rigid building blocks in this structure, reminiscent of our recent findings in a cerium oxalate–formate framework,<sup>[3b]</sup> wherein rigid organic ligands can strongly affect the degree of mechanical anisotropy. More importantly, our results demonstrate that the global anisotropic properties of **1** are determined not only by the underlying pore morphology, but also by the relatively flexible zinc–oxygen cores which permit utilization of the void volume of the channel to accommodate stresses.<sup>[21]</sup>

In summary, this work represents the first study that has combined experimental and computational approaches to establish the structure-mechanical property relationships of an *anisotropic* hybrid framework material, **1**. The elastic anisotropy of **1** has been investigated both in terms of the global chemical topology (i.e. the morphology of the pore), and in terms of its fine structural details (i.e. flexible metal–oxygen environment vs stiff organic ligands<sup>[22]</sup>). An efficient computational scheme has also been introduced to approximate the elastic properties of framework materials. Its validation by nanoindentation measurements and further rationalization by well-established hydrostatic pressure simulations augurs well for future work in this area. Although some discrepancies remain between theory and experiment, it is clear that detailed insight into the fundamental building blocks is made possible only by means of first-principles theory, which will be invaluable to experimentalists in the exploration of both dense and porous MOF materials.

## Acknowledgements

We thank the University of Cambridge and the European Research Council (C.A.M. and A.K.C.) and the Isaac Newton Trust (J.C.T.) for research funding. The authors are grateful to Dr. J. B. Orton, the EPSRC UK National Crystallography Service, and Dr. O. Presly (Oxford Diffraction Applications Laboratory, Yarnton UK) for single-crystal X-ray diffraction data. The computational work was performed on the supercomputer MareNostrum at the Barcelona Supercomputing Center (Centro Nacional de Supercomputación).

**Keywords:** density functional calculations · elastic anisotropy · metal–organic frameworks · mechanical properties · nanostructures

- [1] For an extensive recent overview of the field see: a) *Chem. Soc. Rev.* **2009**, *5*; b) G. Férey, *Chem. Soc. Rev.* **2008**, *37*, 191–214.
- [2] a) A. K. Cheetham, C. N. R. Rao, *Science* **2007**, *318*, 58–59; b) C. N. R. Rao, A. K. Cheetham, A. Thirumurugan, *J. Phys. Condens. Matter* **2008**, *20*, 083202.
- [3] a) J. C. Tan, C. A. Merrill, J. B. Orton, A. K. Cheetham, *Acta Mater.* **2009**, *57*, 3481–3496; b) J. C. Tan, J. D. Furman, A. K. Cheetham, *J. Am. Chem. Soc.* **2009**, *131*, 14252–14254; c) E. C. Spencer, R. J. Angel, N. L. Ross, B. E. Hanson, J. A. K. Howard, *J. Am. Chem. Soc.* **2009**, *131*, 4022–4026; d) D. F. Bahr, J. A. Reid, W. M. Mook, C. A. Bauer, R. Stumpf, A. J. Skula, N. R. Moody, B. A. Simmons, M. M. Shindel, M. D. Allendorf, *Phys. Rev. B* **2007**, *76*, 184106; e) Young's modulus of MIL-101(Cr) framework nanoparticles was determined to be  $17 \pm 10$  GPa: A. Demessence, P. Horcajada, C. Serre, C. Boissière, D. Grosso, C. Sanchez, G. Férey, *Chem. Commun.* **2009**, 7149–7151.
- [4] The bulk modulus (inverse of compressibility) is a measure of volumetric elasticity and indicates the resistance of the material towards hydrostatic compression.
- [5] The Young's modulus is a measure of the material's intrinsic stiffness, and its resistance towards elastic deformation under unidirectional strains.
- [6] Computational studies of the mechanical properties of MOFs are limited to MOF-5 and several other members of the IRMOF family, see: a) Ref. [3d]; b) M. Mattesini, J. M. Soler, F. Yndurain, *Phys. Rev. B* **2006**, *73*, 094111; c) A. Samanta, T. Furuta, J. Li, *J. Chem. Phys.* **2006**, *125*, 084714; d) W. Zhou, T. Yildirim, *Phys. Rev. B* **2006**, *74*, 180301; e) A. Kuc, A. Enyashin, G. Seifert, *J. Phys. Chem. B* **2007**, *111*, 8179; f) S. S. Han, W. A. Goddard, *J. Phys. Chem. C* **2007**, *111*, 15185; g) J. A. Greathouse, M. D. Allendorf, *J. Phys. Chem. C* **2008**, *112*, 5795.
- [7] CCDC 761 446 contains the supplementary crystallographic data for this paper, which can be obtained free of charge from [www.ccdc.cam.ac.uk/data\\_request/cif](http://www.ccdc.cam.ac.uk/data_request/cif).
- [8] For low-symmetry crystals, such as triclinic cell, the derivation of the Young's modulus requires calculation of 21 independent elastic constants of a fourth rank tensor  $C_{ijkl}$ , the accuracy of which directly influences the former. Details of the proposed scheme are given in the SI.
- [9] K. W. Chapman, G. H. Halder, P. J. Chupas, *J. Am. Chem. Soc.* **2009**, *131*, 17546–17547.
- [10] M. Ernzerhof, G. E. Scuseria, *J. Chem. Phys.* **1999**, *110*, 5029.
- [11] For a recent review see: S. Keskin, J. Liu, R. B. Rankin, J. K. Johnson, D. S. Sholl, *Ind. Eng. Chem. Res.* **2009**, *48*, 2355–2371.
- [12] The bulk modulus was calculated according to the stress–strain approach, where cell parameters were optimized at each applied pressure. To avoid discrepancies between electronic structure methods, the bulk modulus of MOF-5 was recalculated with the same scheme and pseudo-potential as in **1**. We found a similar value of 16.6 GPa for MOF-5. See the SI for the full discussion.
- [13] In low-symmetry crystals, the modulus determined by the indenter tip is biased towards the intrinsic modulus lying along its axis. Full details can be found in ref. [3a].

- [14] Finite-temperature simulations have shown that the bulk modulus of MOF-5 decreases from 19.37 GPa at 10 K to 16.66 GPa at 300 K<sup>[6f]</sup> (and in an alternative study from 20.0 to 4 GPa at 0 K and 300 K,<sup>[6g]</sup> respectively) and the elastic constant  $C_{11}$  from 44.53 GPa at 10 K to 34.15 GPa at 300 K.<sup>[6f]</sup>
- [15] a) P. Pulay, *Mol. Phys.* **1969**, *17*, 197–204; b) H. B. Schlegel, *Theor. Chem. Acc.* **2000**, *103*, 294–296.
- [16] a) H. S. Wei, A. Zunger, *Phys. Rev. B* **1988**, *37*, 8958; b) A. Janotti, D. Segev, C. G. Van de Walle, *Phys. Rev. B* **2006**, *74*, 045202.
- [17] a) For a recent highlight in the field, see A. J. Cohen, P. Mori-Sanchez, W. Yang, *Science* **2008**, *321*, 792–794; b) For a review, see S. Kümmel, L. Kronik, *Rev. Mod. Phys.* **2008**, *80*, 3–60.
- [18] Inclusion of the exact exchange, that is, PBE0 level of theory, and DFT+U methodology results in increased band gaps of **1** and ZnO. See the SI for the details.
- [19] The defect-free computational model and small simulation cell results in a linear pressure–volume relationship for **1** over the 0–5 GPa pressure range. Full details are in the SI.
- [20] The pseudo-orthorhombic unit cell is comprised of 168 atoms (8 formula units), corresponding to the size of the  $2 \times 1 \times 2$  triclinic cell.
- [21] A similar conclusion was deduced for the IRMOFs family, that rigid BDC organic linkers are tilted around the Zn–O cores, see ref. [6f].
- [22] The simulations performed at 0 K underestimates the flexibility of the organic ligands. At a finite temperature, rotational fluctuations might lower the stiffness of the phosphonoacetate ligand. The flexibility of the phosphate ligand, however, is expected not to change considerably at ambient conditions.

---

Received: May 6, 2010  
Published online on July 6, 2010